4

Active Control of Human-Induced Vibrations Using a Proof-Mass Actuator

Iván M. Díaz
Universidad de Castilla-La Mancha
Spain

1. Introduction

Advances in structural technologies, including construction materials and design technologies, have enabled the design of light and slender structures, which have increased susceptibility to human-induced vibration. This is compounded by the trend toward open-plan structures with fewer non-structural elements, which have less inherent damping. Examples of notable vibrations under human-induced excitations have been reported in floors, footbridges and grandstands, amongst other structures (Bachmann, 1992; Bachmann, 2002; Hanagan et al., 2003a). Such vibrations can cause a serviceability problem in terms of disturbing the users, but they rarely affect the fatigue behaviour or safety of structures.

Solutions to overcome human-induced vibration serviceability problems might be: (i) designing in order to avoid natural frequencies into the habitual pacing rate of walking, running or dancing, (ii) stiffening the structure in the appropriate direction resulting in significant design modifications, (iii) increasing the weight of the structure to reduce the human influence being also necessary a proportional increase of stiffness and (iv) increasing the damping of the structure by adding vibration absorber devices. The addition of these devices is usually the easiest way of improving the vibration performance. Traditionally, passive vibration absorbers, such as tuned mass dampers (TMDs) (Setareh & Hanson, 1992; Caetano et al., 2010), tuned liquid dampers (Reiterer & Ziegler, 2006) or visco-elastic dampers, etc., have been employed. However, the performance of passive devices is often of limited effectiveness if they have to deal with small vibration amplitude (such as those produced by human loading) or if vibration reduction over several vibration modes is required since they have to be tuned to a single mode. Semi-active devices, such semi-active TMDs, have been found to be more robust in case of detuning due to structural changes, but they exhibit only slightly improved performance over passive TMDs and they still have the fundamental problem that they are tuned to a single problematic mode (Setareh, 2002; Occhiuzzi et al., 2008). In these cases, an active vibration control (AVC) system might be more effective and then, an alternative to traditional passive devices (Hanagan et al., 2003b). A state-of-the-art review of technologies (passive, semi-active and active) for mitigation of human-induced vibration can be found in (Nyawako & Reynolds, 2007). Furthermore, techniques to cancel floor vibrations (especially passive and semi-active techniques) are reviewed in (Ebrahimpour & Sack, 2005) and the usual adopted solutions to cancel footbridge vibrations can be found in (FIB, 2005).

An AVC system based on direct velocity feedback control (DVFC) with saturation has been studied analytically and implemented experimentally for the control of human-induced vibrations via an active mass damper (AMD) (also known as inertial actuator or proof-mass actuator) on a floor structure (Hanagan & Murray, 1997) and on a footbridge (Moutinho et al., 2010). This actuator generates inertial forces in the structure without need for a fixed reference. The velocity output, which is obtained by an integrator circuit applied to the measured acceleration response, is multiplied by a constant gain and feeds back to a collocated force actuator. The term collocated means that the actuator and sensor are located physically at the same point on the structure. The merits of this method are its robustness to spillover effects due to high-order unmodelled dynamics and that it is unconditionally stable in the absence of actuator and sensor (integrator circuit) dynamics (Balas, 1979). Nonetheless, when such dynamics are considered, the stability for high gains is no longer guaranteed and the system can exhibit limit cycle behaviour, which is not desirable since it could result in dramatic effects on the system performance and its components (Díaz & Reynolds, 2010a). Then, DVFC with saturation is not such a desirable solution. Generally, the actuator and sensor dynamics influence the system dynamics and have to be considered in the design process of the AVC system. If the interaction between sensor/actuator and structure dynamics is not taken into account, the AVC system might exhibit poor stability margins, be sensitive to parameter uncertainties and be ineffective. A control strategy based on a phase-lag compensator applied to the structure acceleration (Díaz & Reynolds, 2010b), which is usually the actual magnitude measured, can alleviated such problems. This compensator accounts for the interaction between the structure and the actuator and sensor dynamics in such a way that the closed-loop system shows desirable properties. Such properties are high damping for the fundamental vibration mode of the structure and high stability margins. Both properties lead to a closed-loop system robust with respect to stability and performance (Preumont, 1997). This control law is completed by: (i) a high-pass filter, applied to the output of the phase-lag compensator, designed to avoid actuator stroke saturation due to low-frequency components and (ii) a saturation nonlinearity applied to the control signal to avoid actuator force overloading at any frequency. This methodology will be referred as to compensated acceleration feedback control (CAFC) from this point onwards.

This chapter presents the practical implementation of an AMD to cancel excessive vertical vibrations on an in-service office floor and on an in-service footbridge. The AMD consists of a commercial electrodynamic inertial actuator controlled via CAFC. The remainder of this chapter is organised as follows. The general control strategy together with the structure and actuator dynamic model are described in Section 2. The control design procedure is described in Section 3. Section 4 deals with the experimental implementation of the AVC system on an in-service open-plan office floor whereas Section 5 deals with the implementation on an in-service footbridge. Both sections contain the system dynamic models, the design of CAFC and results to assess the design. Finally, some conclusions are given in Section 6.

2. Control strategy and system dynamics

The main components of the general control strategy adopted in this work are shown in Fig. 1. The output of the system is the structural acceleration since this is usually the most convenient quantity to measure. Because it is rarely possible to measure the system state

and due to simplicity reasons, direct output measurement feedback control might be preferable rather than state-space feedback in practical problems (Chung & Jin, 1998). In this Fig., G_A is the transfer function of the actuator, G is of the structure, C_D is of the direct compensator and C_F is of the feedback compensator. The direct one is merely a phase-lead compensator (high-pass property) designed to avoid actuator stroke saturation for low-frequency components. It is notable that its influence on the global stability will be small since only a local phase-lead is introduced. The feedback one is a phase-lag compensator designed to increase the closed-loop system stability and to make the system more amenable to the introduction of significant damping by a closed-loop control. The control law is completed by a nonlinear element f that is assumed to be a saturation nonlinearity to account for actuator force overloading.

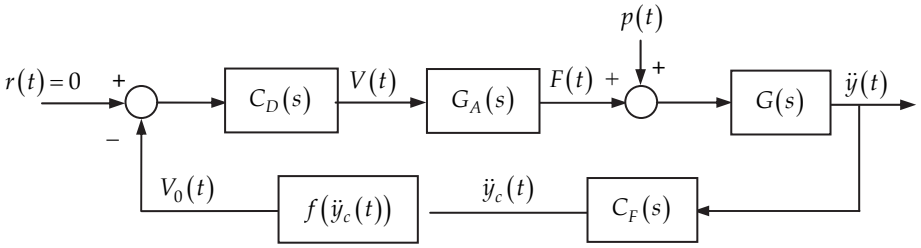

$r(t)$:	Reference command	$\ddot{y}(t)$:	Acceleration response
$V(t)$:	Control voltage	$\ddot{y}_c(t)$:	Compensated acceleration
$F(t)$:	Actuator force	$V_0(t)$:	Initial control voltage
$p(t)$:	Plant disturbance	$f(\ddot{y}_c)$:	Nonlinear element

$C_D(s)$: Transfer function of the direct compensator

$G_A(s)$: Transfer function of the AMD

$G(s)$: Transfer function of the structure

$C_F(s)$: Transfer function of the feedback compensator

Fig. 1. General control scheme

2.1 Structure dynamics

If the collocated case between the acceleration (output) and the force (input) is considered and using the modal analysis approach, the transfer function of the structure dynamics can be represented as an infinitive sum of second-order systems as follows (Preumont, 1997)

$$G(s) = \sum_{i=1}^{\infty} \frac{\chi_i s^2}{s^2 + 2\zeta_i \omega_i s + \omega_i^2}, \tag{1}$$

where $s = j\omega$, ω is the frequency, χ_i, ζ_i and ω_i are the inverse of the modal mass, damping ratio and natural frequency associated to the i-th mode, respectively. For practical application, N vibration modes are considered in the frequency bandwidth of interest. The transfer function G (1) is thus approximated by a truncated one as follows

$$G(s) \simeq \sum_{i=1}^{N} \frac{\chi_i s^2}{s^2 + 2\zeta_i \omega_i s + \omega_i^2} \,. \tag{2}$$

2.2 Proof-mass actuator dynamics

The actuator consists of a reaction (moving) mass attached to a current-carrying coil moving in a magnetic field created by an array of permanent magnets. The linear behaviour of a proof-mass actuator can be closely described as a linear third-order model (Reynolds et al., 2009). That is, a low-pass element is added to a linear second-order system in order to account for the low-pass property exhibited by these actuators. The cut-off frequency of this element is not always out of the frequency bandwidth of interest since it is approximately 10 Hz (APS). Such a low-pass behaviour might affect importantly the global stability of the AVC system. Thus, the actuator is proposed to be modelled by

$$G_A(s) = \left(\frac{K_A s^2}{s^2 + 2\zeta_A \omega_A s + \omega_A^2} \right) \left(\frac{1}{s + \varepsilon} \right) = \frac{K_A s^2}{s^3 + (2\zeta_A \omega_A + \varepsilon) s^2 + (2\zeta_A \omega_A \varepsilon + \omega_A^2) s + \varepsilon \omega_A^2} \tag{3}$$

where $K_A > 0$, and ζ_A and ω_A are, respectively, the damping ratio and natural frequency which take into consideration the suspension system and internal damping. The pole at $-\varepsilon$ provides the low-pass property.

3. Controller design

The purpose of this section is to show a procedure to design the compensators C_D and C_F (see Fig. 1). The design of C_D is undertaken in the frequency domain and the design of C_F is carried out through the root locus technique. The root locus maps the complex linear system roots of the closed-loop transfer function for control gains from zero (open-loop) to infinity (Bolton, 1998). In the design of C_F, it is assumed that the natural frequency of the actuator ω_A (see Eq. (3)) is below the first natural frequency of the structure ω_1 (see Eq. (2)) (Hanagan, 2005).

3.1 Direct compensator

The transfer function between the inertial mass displacement and input voltage to the actuator can be considered as follows

$$G_d(s) = \frac{1}{m_A} \frac{G_A(s)}{s^2}, \tag{4}$$

with m_A being the mass value of the inertial mass. Fig. 2a shows an example of magnitude of G_d. The inertial mass displacement at low frequencies should be limited due to stroke saturation. A transfer function with the following magnitude is defined

$$\left| \hat{G}_d(j\omega) \right| = \begin{cases} d & 0 \le \omega \le \hat{\omega} \\ \left| G_d(j\omega) \right| & \hat{\omega} < \omega < \infty \end{cases}, \tag{5}$$

in which d is the maximum allowable stroke for harmonic input per unit voltage and $\hat{\omega}$ is the higher frequency that fulfils $\left|G_d(j\omega)\right| = d$. A high-pass compensator of the form

$$C_D(s,\lambda,\eta) = \frac{s+\lambda}{s+\eta} \text{ with } \eta > \lambda \geq 0, \tag{6}$$

is applied to the initial control voltage V_0 and its output is the filtered input V to the actuator (see Fig. 1). Fig. 2b shows an example of C_D. The following error function is defined

$$e(\omega,\lambda,\eta) = \left(\left|\hat{G}_d(j\omega)\right| - \left|C_D(j\omega,\lambda,\eta)G_d(j\omega)\right|\right)^2, \tag{7}$$

with $\omega \in (\omega_L, \omega_U)$, $\omega_L < \hat{\omega}$, $\omega_U > \hat{\omega}$, and ω_L and ω_U being, respectively, the lower and upper value of the frequency range that is considered in the design. The lower frequency ω_L must be selected in such a way that the actuator resonance is sufficiently included and the upper frequency ω_U must be chosen so that the structure dynamics that are prone to be excited are included. Parameters λ and η of the compensator are obtained by minimising the error function (7)

$$\min_{(\lambda,\eta)\in\mathbb{R}^+} e(\omega,\lambda,\eta), \forall\omega \in (\omega_L, \omega_U), \tag{8}$$

with $\lambda \in [0, \lambda_{\max})$, $\eta \in [0, \eta_{\max})$, $\lambda_{\max}$, $\eta_{\max} \leq \varepsilon$ and $\lambda_{\max}$ and $\eta_{\max}$ being, respectively, the maximum considered value of λ and η for the optimisation problem (8). Note that λ and η are delimited by the low-pass property of the actuator ε in order to minimise the influence of C_D on the global stability properties. By and large, the objective is to fit $C_D(j\omega)G_d(j\omega)$ to d for $\omega_L < \omega < \hat{\omega}$ and not to affect the dynamics for $\hat{\omega} < \omega < \omega_U$ (see Fig. 2a). The result is a high-pass compensator that introduces dynamics mainly in the frequency range $\omega_L < \omega < \hat{\omega}$ in such a way that the global stability is not compromised.

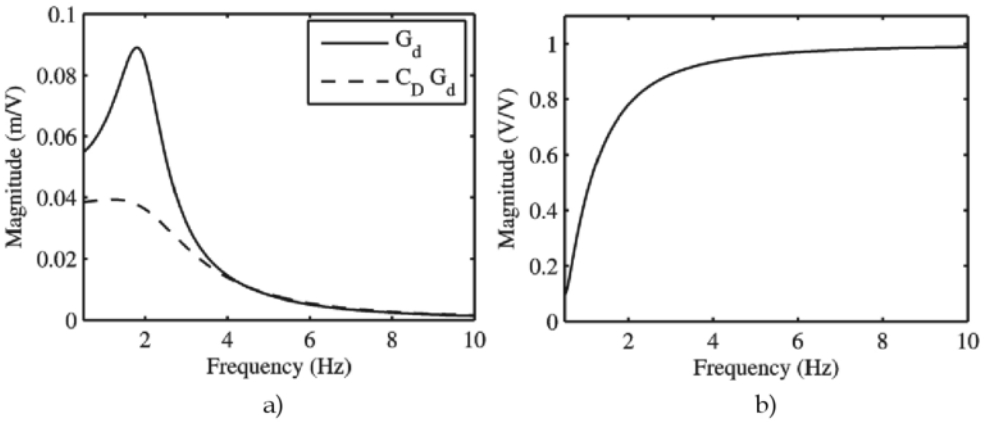

Fig. 2. Effect of the high-pass compensator on the actuator dynamics. a) Magnitude of G_d and $C_D G_d$. b) Magnitude of C_D

3.2 Feedback compensator

To illustrate the selection of the form of the compensator C_F, the root locus map (s-plane) for four different cases is shown in Fig. 3. A realistic structure is assumed with two significant vibration modes. The modal mass and damping ratio for both modes are assumed to be 20 tonnes and 0.03, respectively. The four cases are: a) direct acceleration feedback control (DAFC) considering two vibration modes at 4 and 10 Hz, respectively; b) DVFC for the same structure as in a); c) DAFC considering two vibration modes at 7 and 10 Hz, respectively; and d) DVFC for the same structure as in c). The actuator dynamics (Eq. (3)) is represented by a pair of high-damped poles, two zeros at the origin and a real pole and the structure is represented by two zeros at the origin and interlacing low-damped poles and zeros. It is clearly shown that the resulting root locus has non-collocated system features due to the influence of the actuator dynamics on the structure dynamics. That is, when the actuator dynamics are considered, the interlacing pole-zero pattern exhibited by collocated systems is

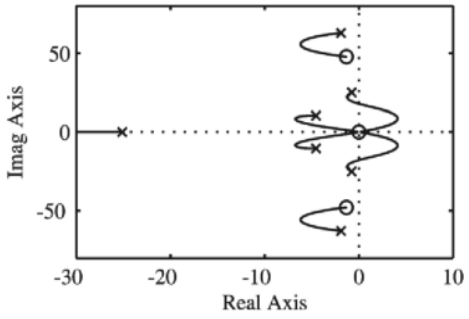

DAFC	
First frequency	4 Hz
Second frequency	10 Hz
Maximum damping	0.047

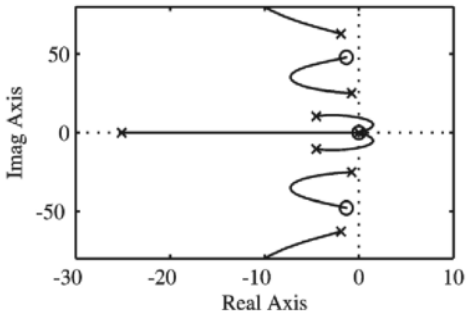

DVFC	
First frequency	4 Hz
Second frequency	10 Hz
Maximum damping	0.205

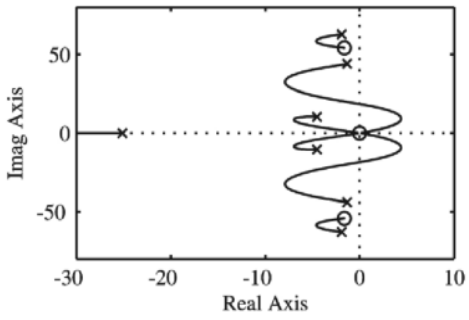

DAFC	
First frequency	7Hz
Second frequency	10 Hz
Maximum damping	0.242

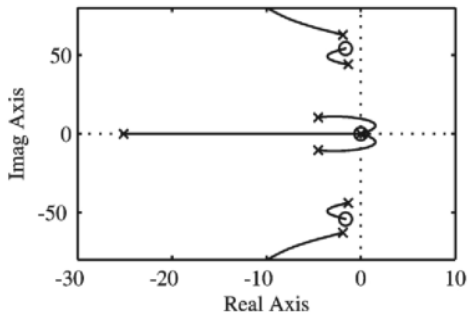

DVFC	
First frequency	7Hz
Second frequency	10 Hz
Maximum damping	0.070

Fig. 3. Examples of root loci. (×) poles; (o) zeros

no longer accomplished. On one hand, it is observed that for a structure with a fundamental frequency of 4 Hz, direct output feedback (DAFC since the actual measurement is the acceleration) will provide very small relative stability (the distance of the poles to the imaginary axis in the s-plane) and low damping (Bolton, 1998). However, the inclusion of an integrator circuit (a pole at the origin for an ideal integrator), which results in DVFC, improves substantially such properties. On the other hand, for a structure with a higher fundamental frequency (7 Hz), DAFC provides much better features than DVFC.
Fig. 3 shows the fact that DVFC might not be a good solution and supports the use of CAFC. It is applied the following phase-lag compensator to the measured acceleration

$$C_F(s)=\frac{s+\gamma}{s} \text{ with } \gamma \geq 0 . \tag{9}$$

If $\gamma = 0$, the control scheme will be DAFC since $C_F(s)=1$. If $\gamma \gg \varepsilon$, which means that the zero of the compensator does not affect the dominant system dynamics, the control scheme will then be considered DVFC. Parameter γ has to be chosen according to the closed-loop poles corresponding to the fundamental frequency of the structure in order to: 1) improve substantially their relative stability, 2) decrease their angles with respect to the negative real axis to allow increasing damping, and 3) increase the distance to the origin to allow increasing natural frequency. Note that increasing values both of the frequency and the damping result in decreasing the settling time of the corresponding dynamics (Bolton, 1998). The possible values of γ that provide the aforementioned features can be bound through the departure angle at zero gain of the locus corresponding to the fundamental structure vibration mode. This angle must point to negative values of the real axis. To obtain this angle, the argument equation of the closed-loop characteristic equation is used. That is, any point s_1 of a specific trajectory verifies the following equation

$$\sum_{i=1}^{n_z}\angle(s_1+z_i)-\sum_{j=1}^{n_p}\angle(s_1+p_j)=\pm(2k+1)\pi \text{ with } k\in\mathbb{N} , \tag{10}$$

in which n_z is the number of zeros, n_p is the number of poles and $\angle(s_1+z_i)$ and $\angle(s_1+p_j)$ are the angles of vectors drawn from the zeros and poles, respectively, to point s_1. The departure angle can be determined by letting s_1 be a point very close to one of the poles of the fundamental structure vibration mode. As an example, the dominant dynamics are considered without the direct compensator. Fig. 4 shows the map of zeros and poles under the aforementioned conditions. Eq. (10) can be written as follows

$$(\beta_1+\beta_2+\beta_3+\beta_4)-(\alpha_1+\alpha_2+\alpha_3+\alpha_4+\alpha_5)=\pm(2k+1)\pi \text{ with } k\in\mathbb{N} . \tag{11}$$

If it is considered that the damping of the fundamental vibration mode is $\zeta_1 \simeq 0$, the following assumptions can be done: $\beta_1=\beta_2=\beta_3\simeq\pi/2$ and $\alpha_5\simeq\pi/2$. Therefore, Eq. (11) can be rewritten as

$$\beta_4-(\alpha_1+\alpha_2+\alpha_3+\alpha_4)=\pm 2k\pi \text{ with } k\in\mathbb{N} . \tag{12}$$

Considering transfer functions (2) and (3), the angles α_1, α_2 and α_3 are of the following form

$$\alpha_1 = \text{atan}\left(\frac{\omega_1}{\varsigma_A\omega_A} - \frac{\sqrt{1-\varsigma_A^2}}{\varsigma_A}\right),\ \alpha_2 = \text{atan}\left(\frac{\omega_1}{\varsigma_A\omega_A} + \frac{\sqrt{1-\varsigma_A^2}}{\varsigma_A}\right),\ \text{and}\ \alpha_3 = \text{atan}\left(\frac{\omega_1}{\varepsilon}\right) \tag{13}$$

Considering transfer functions (2) and (9), the angle β_4 is obtained as

$$\beta_4 = \text{atan}\left(\frac{\omega_1}{\gamma}\right) \tag{14}$$

Then, by imposing a minimum $\alpha_{4,\min}$ and a maximum $\alpha_{4,\max}$ value of the departure angle α_4 of the fundamental structure vibration mode, a couple of values of β_4 can be obtained

$$\beta_{4,\min} = -2\pi + \left(\alpha_1 + \alpha_2 + \alpha_3 + \alpha_{4,\min}\right),\ \beta_{4,\max} = -2\pi + \left(\alpha_1 + \alpha_2 + \alpha_3 + \alpha_{4,\max}\right) \tag{15}$$

in which it is assumed $k = 1$. Therefore, the variation interval of β_4 is derived as follows

$$\beta_4 \in \left(\max\left(0;\beta_{4,\min}\right),\ \min\left(\pi/2;\beta_{4,\max}\right)\right) \tag{16}$$

and using Eq. (14), the corresponding variation interval of $\gamma \in \left(\gamma_{\min},\gamma_{\max}\right)$ is determined. The final value of γ must be chosen so that the attractor properties of the zero are focussed on the fundamental vibration mode.

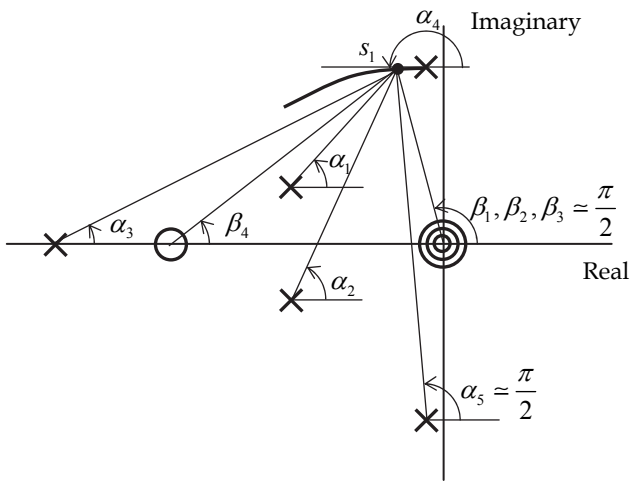

Fig. 4. Departure angle of the locus corresponding to the fundamental structure vibration mode (not to scale). (×) pole; (o) zeros

3.3 Stability

Stability is the primary concern in any active control system applied to civil engineering structures, mainly due to safety and serviceability reasons. The control scheme of Fig. 1, assuming that the nonlinear element *f* is a saturation nonlinearity, is analysed in this section. The nonlinear element can be written as

$$f\left(\ddot{y}_c(t)\right)=\begin{cases} K_c\ddot{y}_c(t) & \left|\ddot{y}_c(t)\right|\le V_s/K_c \\ V_s sign\left(\ddot{y}_c(t)\right) & \left|\ddot{y}_c(t)\right|> V_s/K_c \end{cases} \tag{17}$$

where K_c is the control gain and V_s is the maximum allowable control voltage to the actuator (saturation level). The saturation nonlinearity is introduced to avoid actuator force saturation and to keep the system safe under any excitation and independently of selection of control parameters. The stability can be studied using the Describing Function (DF) tool in its basic form (Slotine & Li, 1991). Firstly, the total transfer function of the linear part (Eqs. (2), (3), (6) and (9)) is obtained (see Fig .1)

$$G_T\left(j\omega\right)=C_D\left(j\omega\right)G_A\left(j\omega\right)G\left(j\omega\right)C_F\left(j\omega\right). \tag{18}$$

Then, from the root locus of G_T, the limit gain $K_{c,\text{limit}}$ for which the closed-loop system becomes unstable is derived. This is the minimum value of the control gain K_c (see Eq. (17)) for which at least one of the loci intersects the imaginary axis.

Secondly, the DF, denoted by $N(A,\omega)$, for the nonlinear element is obtained. The DF is the ratio between the fundamental component of the Fourier series of the nonlinear element output and a sinusoidal input given by $x(t)=A\sin(\omega t)$. If the nonlinearity is hard, odd and single-valued (the case of saturation nonlinearity), the DF depends only on the input amplitude $N(A,\omega)=N(A)$, i.e., it is a real function. The DF for a saturation nonlinearity is (Slotine & Li, 1991)

$$N(A)=\begin{cases} K_c & A\le a \\ \dfrac{2K_c}{\pi}\left[\arcsin\left(\dfrac{a}{A}\right)-\dfrac{a}{A}\sqrt{1-\dfrac{a^2}{A^2}}\right] & A>a \end{cases} \tag{19}$$

with $a=V_s/K_c$ (see Eq. (17)). The normalised DF $N(A)/K_c$ (19) is plotted in Fig. 5a as a function of A/a. If the input amplitude is in the linear range $(A\le a)$, $N(A)$ is constant and equal to the control gain $N(A)=K_c$. $N(A)$ then decreases as the input amplitude increases when $A>a$. That is, saturation does not occur for small signals and it reduces the ratio of the output to input as the input increases.

Thirdly, the extended Nyquist criterion using the DF is applied

$$G_T\left(j\omega\right)=-1/N(A). \tag{20}$$

Each solution of Eq. (20) predicts a limit cycle behaviour (self-sustained periodic undesirable vibration). The total transfer function $G_T\left(j\omega\right)$ will intersect the real axis at $-1/K_{c,\text{limit}}$. With regards to the plot of $-1/N(A)$, it will start at $-1/K_c$ and go to $-\infty$ as A increases. Depending on the value of K_c, both plots $G_T\left(j\omega\right)$ and $-1/N(A)$ can intersect. Fig. 5b illustrates this fact. The conclusion is that: if $K_c<K_{c,\text{limit}}$, the system is asymptotically stable and goes to zero vibration (no intersection); otherwise, a limit cycle is predicted (intersection). Such a limit cycle is deduced to be stable by using the limit cycle stability criterion (Slotine & Li, 1991; Díaz & Reynolds, 2010a). The properties of the limit cycle, frequency and amplitude, can be obtained by Eq. (20) particularised to the intersection point.

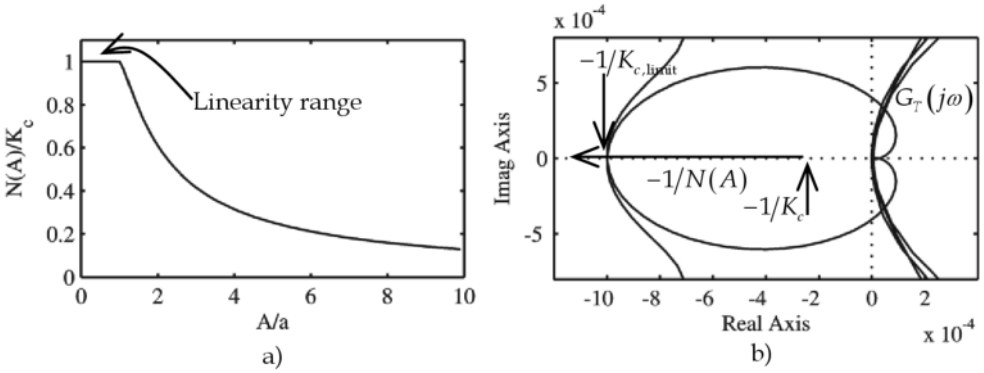

Fig. 5. a) DF for the saturation nonlinearity. b) Nyquist diagram of $G_T(j\omega)$ and $-1/N(A)$

3.4 Design process

The design process of the control scheme represented in Fig. 1 can be summarised in the following steps:

Step 1: Identify the actuator G_A and structure dynamics G.

Step 2: Design the direct compensator (phase-lead) C_D accounting for the actuator stroke saturation. This design is carried out following the procedure described in Subsection 3.1.

Step 3: Design the feedback (phase-lag) compensator C_F to increase the damping and robustness with respect to stability and performance of the closed-loop system by following Subsection 3.2.

Step 4: Design the nonlinear element f according to stability and performance. If f is a saturation nonlinearity, take a saturation value to avoid actuator force overloading and select a suitable gain K_c using the root locus method.

4. Implementation on a floor structure

This Section presents the design and practical implementation of an AVC system based on the procedure presented in Section 3 on an in-service open-plan office floor sited in the North of England.

4.1 Structure description and modal properties

The test structure is a composite steel-concrete floor in a steel frame office building. A plan of the floor is shown in Fig. 6a, in which the measurement points used for the experimental modal analysis (EMA) are indicated. Columns are located along the two sides of the building (without point numbers) and along the centreline (18-27-end), at every other test point (TP) location (i.e, 18, 20, 22, etc.). Fig 6b shows a photograph from TP 44 towards TP 28 and Fig. 6c shows a photograph from TP 12 towards TP 01. The EMA of this structure is explained in detail in (Reynolds et al., 2009). The floor is considered by its occupants to be quite lively, but not sufficiently lively to attract complaints. Special attention is paid to TP 04 (see Fig. 6a) and its surroundings because it is perceived to be a particularly lively location on the floor. Because the vibration perception is particularly acute at this point, this is the candidate for the installation of the AVC system.

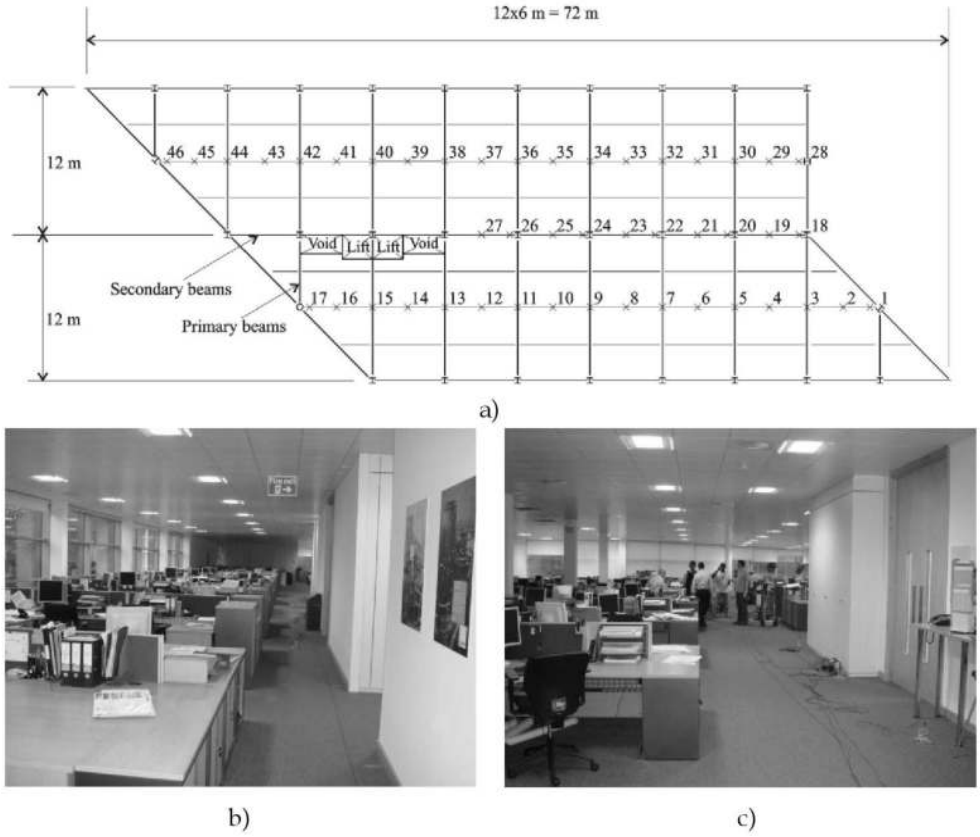

Fig. 6. Floor structure. a) Plan of the floor (not to scale); (×) measurement point used in the EMA. b) View from TP 44 towards TP 28. c) View from TP 12 to TP 01

A multi-input multi-output modal testing is carried out with four excitation points placed at TPs 04, 07, 31 and 36 and responses measured at all TPs. The artificial excitation is supplied by APS Dynamics Model 400 electrodynamic shakers (Fig. 7b) and responses are measured by QA750 force-balance accelerometers (Fig. 7c). Fig 7a shows a photograph of the multishaker modal testing carried out. Fig. 8 shows the magnitudes of the point accelerance FRFs acquired. Interestingly, the highest peak occurs at TP 04 at approximately 6.4 Hz, which is the point on the structure where the response has been subjectively assessed to be highest. Parameter estimation is carried out using the multiple reference orthogonal polynomial algorithm already implemented in ME'scope suite of software. Fig. 9 shows the estimated vibration modes which are dominant at TP 04.

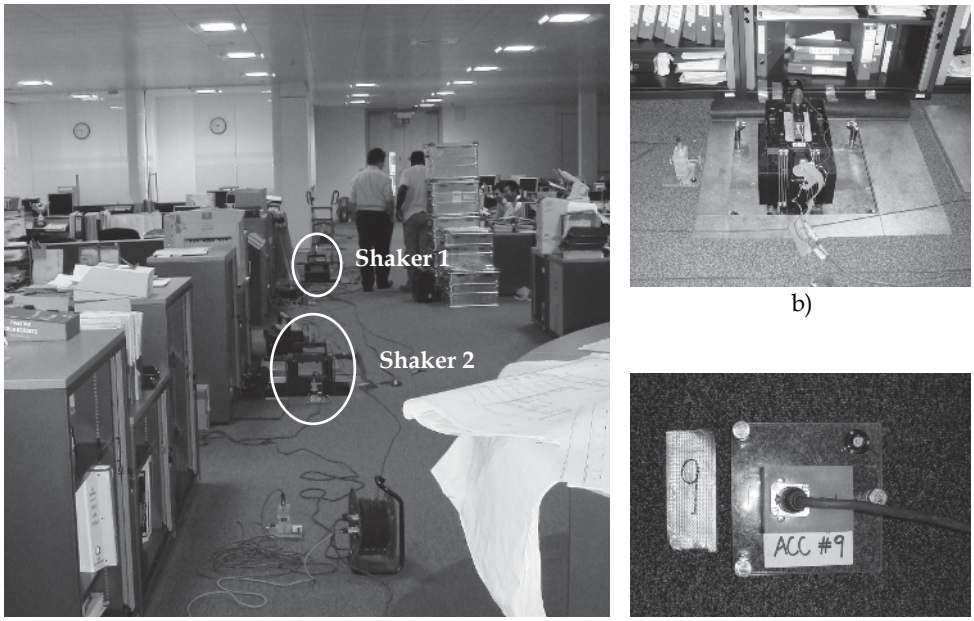

Fig. 7. a) Multishaker modal testing of the floor structure. b) APS Dynamics Model 400 electrodynamic shaker. c) QA750 force-balance accelerometer

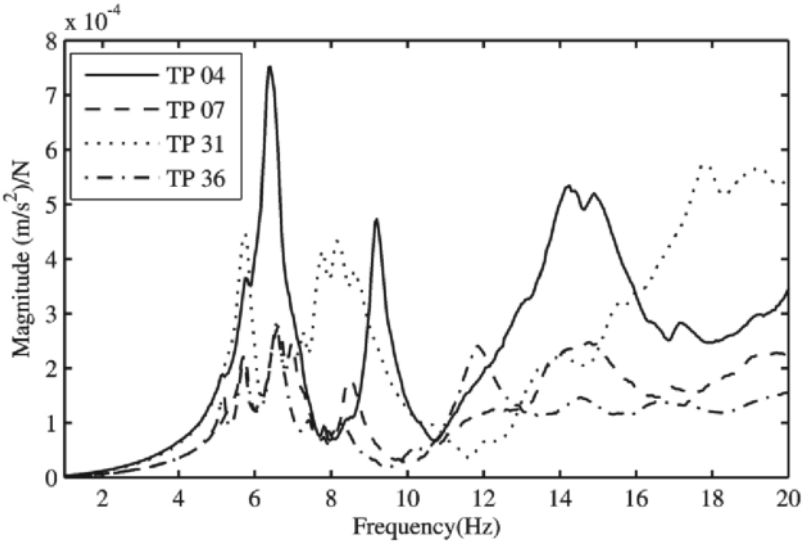

Fig. 8. Magnitudes of the point accelerance FRFs at TP 04, 07, 31 and 36

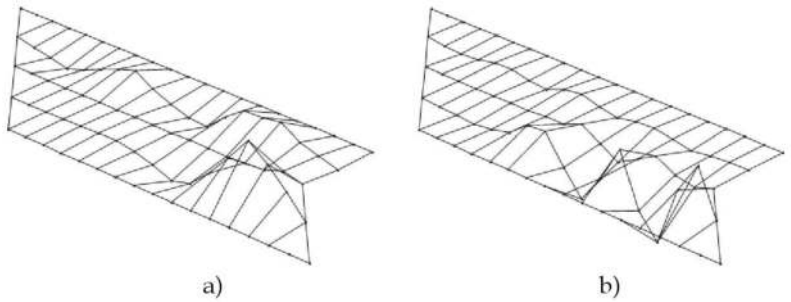

Fig. 9. Estimated vibration modes prone to be excited by human walking at TP 04. a) Vibration mode at 6.37 Hz. b) Vibration mode at 9.19 Hz

4.2 System dynamics

The AVC system is placed at TP 04. The floor dynamics at the AVC location (Eq. (2)) and the actuator dynamics (Eq. (3)) are identified. Using the modal parameters obtained from the EMA, the transfer function of the floor is modelled considering three vibration modes $N = 3$ in the frequency range of 0–20 Hz

$$G(s) = \frac{4.49 \cdot 10^{-5} s^2}{s^2 + 2.36s + 1627} + \frac{1.74 \cdot 10^{-5} s^2}{s^2 + 2.09s + 3341} + \frac{1 \cdot 10^{-4} s^2}{s^2 + 17.59s + 7738} \tag{21}$$

The inertial actuator is an APS Dynamics Model 400 electrodynamic shaker (operated in inertial mode and driven using voltage mode) with an inertial mass of $m_A = 30.4$ kg (APS Manual). The actuator model is obtained to be

$$G_A(s) = \frac{12600 s^2}{s^3 + 62.16 s^2 + 728.6 s + 6573}. \tag{22}$$

The natural frequency of the actuator is estimated as 1.80 Hz and the pole that provides the low pass property is estimated to be $\varepsilon = 50.26$ rad/s (Eq. (3)).

4.3 Controller design

Compensators C_D and C_F are obtained following Section 3. Firstly, C_D is obtained. From (22), the transfer function G_d (Eq. (4)) is derived. By assuming a value of $d = 0.05$ m, which is appropriate considering the actual stroke limit of the actuator is 0.075 m, its magnitude $\left|\hat{G}(j\omega)\right|$ (Eq. (5)) is obtained with $\hat{\omega} = 14.74$ rad/s. The compensator parameters are thus derived from the optimisation problem (8) in which it is assumed $\omega_L = 1.25$ rad/s, $\omega_U = 62.83$ rad/s and $\lambda_{\max} = \eta_{\max} = \varepsilon = 50.26$. The control parameters are then found to be $\lambda = 6.87$ and $\eta = 14.34$.

Secondly, the feedback compensator C_F (Eq. (9)) is obtained. Taking into account the dominant dynamics: G_A, C_D and the fundamental floor vibration mode of (21) (the first one of the three considered mode), and restricting the departure angle of the locus corresponding to the structure vibration mode as $\alpha_4 \in (180, 225)$ deg (see Fig. 4), then the angle corresponding to the zero of the compensator β_4 can be bounded. It is obtained

$\beta_4 \in (10.24, 55.24)$ deg and consequently $\gamma \in (27.9, 223.2)$ using Eq. (14). A value of $\gamma = 55$ is chosen since it must be higher than the inferior limit but it should not be so high that the attractor effect of the zero is focussed on the fundamental vibration mode. The root locus technique is used here. The root locus of G_T (Eq. (18)) for CAFC is plotted in Fig. 10. It can be observed that the linear system might be critically damped for the fundamental floor vibration mode.

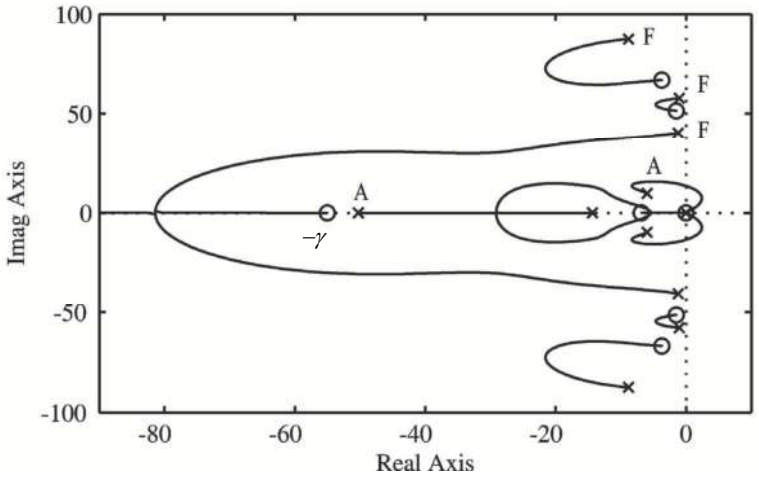

Fig. 10. Root locus of the total transfer function G_T for CAFC. (×) pole; (o) zero; (F) floor; (A) actuator

Finally, the nonlinear element is chosen as a saturation nonlinearity (17) with $V_s = 1$ V, which is a convenient value to avoid actuator force overloading at any frequency of the excitation. Therefore, the stability is guaranteed just by taking a safe control gain $K_c < K_{c,\text{limit}}$. The limit gain is predicted to be $K_{c,\text{limit}} = 44.4$ V/(m/s^2). Values of damping of the actuator poles smaller than 0.30 are not recommended (Hanagan, 2005). This damping is reached for $K_c = 18.6$ V/(m/s^2).

A digital computer is used for the on-line calculation of the control signal V. The system output is sampled with a period $\Delta t = 0.001$ s and the control signal is calculated once every sampling period. Then, the discrete-time control signal is converted into a zero-order-hold continuous-time signal. Likewise, the continuous transfer functions of the compensators are converted to discrete transfer function using the zero-order-hold approximation. Note that the sampled period used is sufficiently small to not consider the delay introduced by the digital implementation of the control scheme.

4.4 Results

The AVC system is assessed firstly by carrying out several simulations using different values of the control gain K_c. MATLAB/Simulink is used for this purpose. The control scheme shown in Fig. 1 is simulated using the transfer function models of the compensators given by Eqs. (6) and (9) with the parameters obtained in Section 4.3 and Eqs. (21) and (22)

obtained from FRF identifications. The control scheme is perturbed by a real walking excitation obtained from an instrumented treadmill (Brownjohn et al., 2004) ($p(t)$ in Fig. 1). Table 1 shows the results obtained. Two different pacing frequencies (1.58 and 2.12 Hz) are used in such a way that the first floor vibration mode might be excited by the third or the fourth harmonic. The results are compared in terms of the maximum transient vibration value (MTVV) calculated from the 1 s running RMS acceleration and from the vibration dose value (VDV) obtained from the total period of the excitation (BS 6472, 2008). The BS 6841 W_b weighted acceleration is used for both measures (BS 6841, 1987). The results predicted that the AVC are quite insensitive to the gain value. The reduction in vibration is approximately 60 % for slow walking (1.58 Hz) and 53 % for fast walking (2.12 Hz) in terms of MTVV. The results in terms of the VDV provide similar reductions as for the MTVV.

Control gain (V/(m/s²))	Uncontrolled	5	10	15	20
Walking at 1.58 Hz					
MTVV(1) (m/s²)	0.030	0.0122	0.0115	0.0115	0.0116
Reduction MTVV (%)	—	59	62	62	61
VDV(2) (m/s$^{1.75}$)	0.063	0.029	0.027	0.027	0.027
Reduction VDV (%)	—	55	58	58	57
Walking at 2.12 Hz					
MTVV (m/s²)	0.033	0.0154	0.0150	0.0156	0.0160
Reduction MTVV (%)	—	53	55	53	52
VDV (m/s$^{1.75}$)	0.073	0.034	0.032	0.033	0.033
Reduction VDV (%)	—	54	56	55	55

Table 1. Simulation performance assessment for the floor structure using several control gains and walking excitation. (1) Maximum Transient Vibration value defined as the maximum value of 1s running RMS acceleration. (2) Cumulative Vibration Dose Value

Actual walking tests are carried out on the test structure using the same walking excitation frequencies as in the simulations. The walking path consists of walking from TP 01 to TP 09 and then back from TP 09 to TP 01 (see Fig. 6). A gain of $K_c = 15\ \mathrm{V}/\left(\mathrm{m/s^2}\right)$ is found to give good performance so that is used in the experiments. Fig. 11 shows BS 6841 W_b weighted response time histories (including the 1s RMS and the cumulative VDV), uncontrolled and controlled, for a pacing frequency of 1.58 Hz, which is controlled using a metronome set to 95 beats per minute (bpm). The MTVV is reduced from $0.031\ \mathrm{m/s^2}$ to $0.010\ \mathrm{m/s^2}$, a reduction of 68 %, and the VDV is reduced from $0.050\ \mathrm{m/s^{1.75}}$ to $0.019\ \mathrm{m/s^{1.75}}$, a reduction of 62 %. The same test is carried out for a pacing frequency of 2.12 Hz (127 bpm). The achieved reduction in terms of the MTVV is now 52 %, from $0.033\ \mathrm{m/s^2}$ to $0.016\ \mathrm{m/s^2}$, and in terms of the VDV is 51 %, from $0.057\ \mathrm{m/s^{1.75}}$ to $0.028\ \mathrm{m/s^{1.75}}$. The experimental reductions agreed very well with the numerical predictions (see Table 1).

Continuous whole-day monitoring has been carried out to assess the vibration reduction achieved by the AVC system. The acceleration is measured from 6:00 am to 6:00 pm during four working days, two without and two with the AVC system. The R-factor is used to quantify the vibration reduction. This factor is defined as the ratio between the 1 s running RMS of the BS 6841 W_b weighted acceleration response and 0.005 m/s² (Wyatt, 1989). Fig. 12 shows the percentage of time during which the R-factor is over 1, 2, 3, 4 and 5. The values

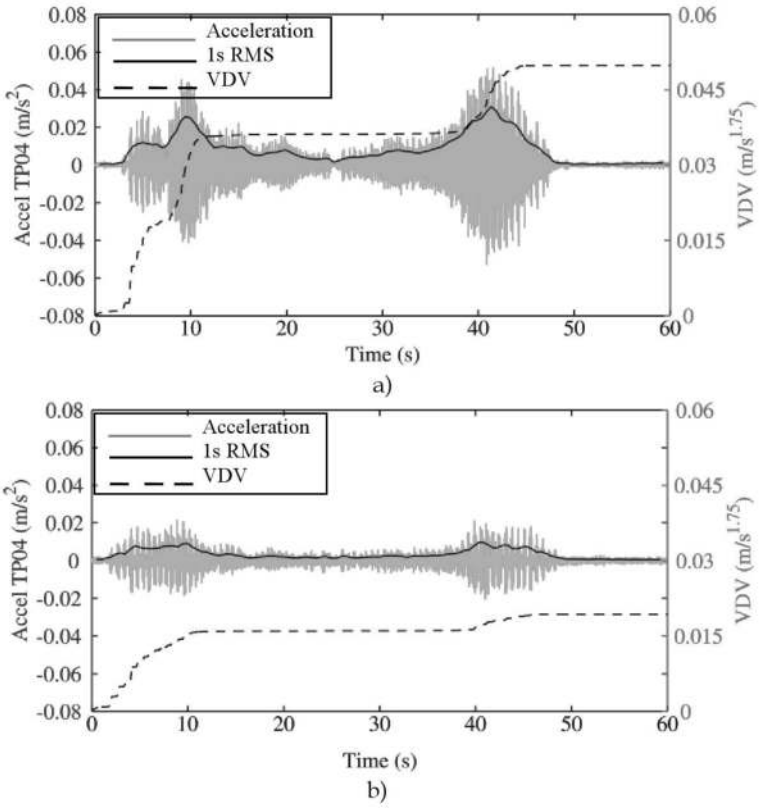

Fig. 11. Experimental results on the floor structure. Walking at 1.58 Hz (95 bpm). a) Uncontrolled $MTVV = 0.031\ m/s^2$ and $VDV = 0.050\ m/s^{1.75}$. b) Controlled $MTVV = 0.010\ m/s^2$ and $VDV = 0.019\ m/s^{1.75}$

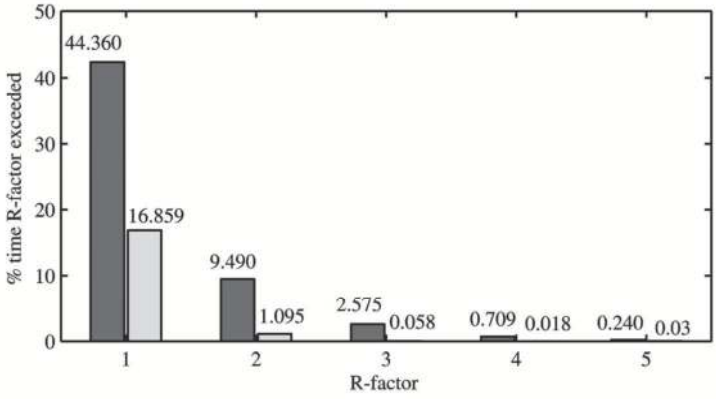

Fig. 12. Whole-day monitoring: percentage of time of exceedance of R-factors

shown in the Fig. are the mean values between the two corresponding days. It is observed that the time for which the R-factor is over 1 is reduced by 60 % and the time for which it is over 4 is significantly reduced by over 97 %. Note that the second reduction is very important since an R-factor of 4 is a commonly used vibration limit for a high quality office floor (Pavic & Willford, 2005). Hence, these results clearly illustrate the effectiveness of the AVC system designed. In addition, the cumulative VDV is also calculated for the same exposure to vibration and using the W_b weighted acceleration. The VDV obtained when the AVC system is disconnected is 0.162 $m/s^{1.75}$ whereas such a value is 0.101 $m/s^{1.75}$ when the system is engaged. The reduction achieved is almost 40 %. Note that the VDV is much more strongly influenced by vibration magnitude than duration (BS 6472, 2008). This fact results in less vibration reduction in terms of the VDV than using the MTVV.

5. Implementation on a footbridge

This Section presents the design and practical implementation of an AVC system based on the procedure presented in Section 3 on an in-service footbridge sited in Valladolid (Spain).

5.1 Structure description and modal properties

The test structure, sited in Valladolid (Spain), is a footbridge that creates a pedestrian link over The Pisuerga River between the Science Museum and the city centre (see Fig. 13). This bridge, built in 2004, is a 234 m truss structure composed of four spans: three made of tubular steel beams and one made of white concrete, all of them with a timber walkway. The main span (Span 3 in Fig. 1), post-tensioning by two external cable systems (transversal and longitudinal), is 111 m, the second span (Span 2 from this point onwards) is 51 m and the other two spans are shorter and stiffer (Gómez, 2004). The external cable systems of Span 3 has both aesthetical reasons (the original design by the architect José Rafael Moneo was based on the form of a fish basket) and structural reasons (making Span 3 stiffer).
Because of its slenderness, this footbridge, especially Span 2, represents a typical lightweight structure sensitive to dynamic excitations produced by pedestrians. Annoying levels of vibration are sometime perceived in Span 2. Special attention is paid to the point of maximum amplitude of the first bending mode (close to mid-span) since the vibration perception is acute at this point, particularly when runners cross the bridge. Therefore, it is decided to study the dynamic properties of this span and implement the AVC system at that point.

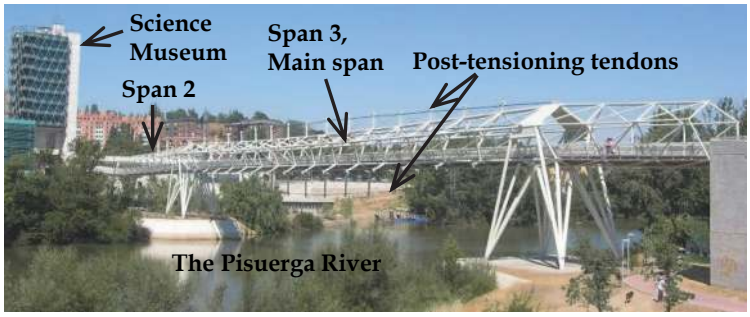

Fig. 13. General view of the Valladolid Science Museum Footbridge

The operational modal analysis of Span 2 is carried out in order to obtain the natural frequencies, damping ratios and modal shapes of the lower vibration modes. The analysis is carried out with five roving and two reference accelerometers. Preliminary spectral analyses and time history recordings indicates that the vertical vibration is considerably higher than the horizontal one, thus, only vertical response measurements are performed. A measurement grid of 3 longitudinal lines with 9 equidistant test points is considered, resulting in 27 test points. Five setups with an acquisition time of 720 seconds and a sampling frequency of 100 Hz are recorded. Thus, it is expected to successfully identify vibration modes up to 30 Hz. The modal parameter estimation is carried out using the ARTeMIS suite of software. In particular, frequency domain methods (Frequency domain decomposition-FDD, enhanced frequency domain decomposition-EFDD and curve-fit frequency domain decomposition-CFDD) are used. Table 2 shows the modal parameters estimated through the modal analysis for the first four vibration modes. Fig. 14 shows the corresponding estimated modal shapes.

		Mode 1	Mode 2	Mode 3	Mode 4
FDD	Frequency (Hz)	3.516	6.250	7.373	9.351
	Damping ratio (%)	—	—	—	—
EFDD	Frequency (Hz)	3.506	6.278	7.386	9.365
	Damping ratio (%)	0.7221	0.4167	0.6571	0.5528
CFDD	Frequency (Hz)	3.508	6.274	7.389	9.367
	Damping ratio (%)	0.7984	0.2599	0.4319	0.3869

Table 2. Natural frequencies and damping ratios identified by the operational modal analysis of the footbridge

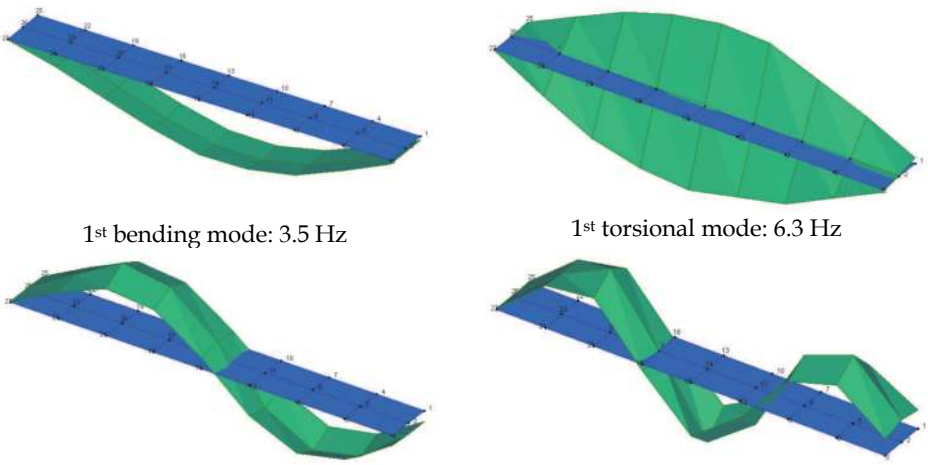

1st bending mode: 3.5 Hz

1st torsional mode: 6.3 Hz

2nd bending mode: 7.4 Hz

3rd bending mode: 9.4 Hz

Fig. 14. Estimated modal shapes for the footbridge structure

5.2 System dynamics

The FRF between the structure acceleration and the input force is obtained at the middle of the transversal steel beam sited closest to the point of maximum value of the first vibration mode (close to mid-span). A chirp signal with frequency content between 1 and 15 Hz is used to excite the first vibration modes. The force is generated by an APS Dynamics Model 400 electrodynamic (as was used for the floor) and the structure acceleration is measured by a piezoelectric accelerometer (as those used for the modal analysis). The force induced by the shaker is estimated by measuring the acceleration of the inertial mass and multiplying this by the magnitude of the inertial mass (30.4 kg). Thus, the structure dynamics for the collocated case between the acceleration (output) and the force (input) can be identified from model (2) as follows

$$G(s) = \frac{5.40 \cdot 10^{-5} s^2}{s^2 + 0.3079 s + 483.6} + \frac{5.85 \cdot 10^{-5} s^2}{s^2 + 0.5887 s + 3451} \tag{23}$$

The vibration modes at 6.3 and 7.4 Hz (see Fig. 14) are not clearly observed and they are not included into this model. The same shaker that is used to obtain the FRF for the structure is used as inertial actuator. The transfer function between the output force and the input voltage is the one given by Eq. (22).

5.3 Controller design

The design process shown in Section 3 is now followed. The direct compensator of the form of (6) is assumed. Again, a maximum stroke for harmonic excitation of d = 0.05 m is considered in the design. The compensator parameters are obtained from the optimisation problem (8) using the parameter used in Subsection 4.3. The controller parameters are found to be $\lambda = 5.6$ and $\eta = 24.6$. These parameters are selected in such a way that the likelihood of stroke saturation is reduced significantly. The stroke saturation leads to collisions of the inertial mass with its stroke limits, imparting highly undesirable shocks to the structure and possibly causing damage to the actuator.

Once the direct compensator is designed, the feedback one (9) is designed considering the dynamics of the actuator, structure and the direct compensator dynamics. As in Subsection 4.3, the departure angle of the locus corresponding to the structure vibration mode is restricted to $\alpha_4 \in (180, 225)$ deg (see Fig. 4). It is obtained $\gamma \geq 35.5$. A value of $\gamma = 50$ is finally chosen. The root locus technique is now used. The root locus of the total transfer function of the linear part (18) is plotted in Fig. 15 (only the dominant dynamics are shown). It is observed that a couple of branches in the root locus corresponding to the actuator dynamics go to the right-half plane provoking unstable behaviour in the actuator. The gain for which the control system is unstable is the limit gain $K_{c,\text{limit}} = 82 \ \text{V}/\left(\text{m}/\text{s}^2\right)$. Finally, a gain of $K_{c,\text{limit}} = 40 \ \text{V}/\left(\text{m}/\text{s}^2\right)$ is chosen. The saturation level is set to $V_s = 1$ V.

5.4 Results

Once both compensators and the control parameters are selected, simulations are carried out in order to assess the AVC performance. MATLAB/Simulink is again used for this purpose. Table 3 shows controlled acceleration response for walking and running excitation. Moreover, the AMD displacement estimation is included.

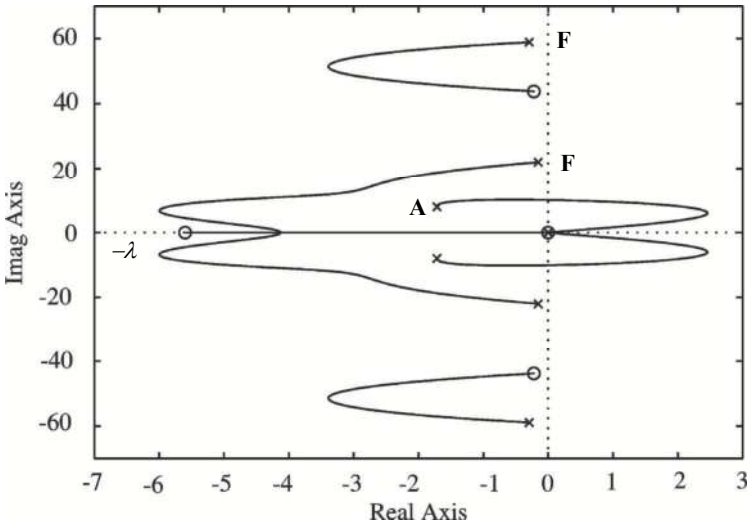

Fig. 15. Root locus of the total transfer function G_T for CAFC on the footbridge. (×) pole; (o) zero; (F) footbridge; (A) actuator

	Uncontrolled (m/s^2)	Controlled (m/s^2)	Reduction (%)	Mass displacement (m)
Walking at 1.75 Hz	0.39	0.04	89	± 0.034
Running at 3.50 Hz	6.16	3.75	40	± 0.022

Table 3. Simulation performance assessment for the footbridge using the peak acceleration for walking and running excitation

Walking and running tests are carried out to assess the efficacy of the AVC system. The walking tests consist of walking at 1.75 Hz such that the first vibration mode of the structure (3.5 Hz) could be excited by the second harmonic of walking. A frequency of 3.5 Hz is used for the running tests so that the structure is excited by the first harmonic of running. The walking/running tests consisted of walking/running from one end of Span 2 to the other and back again. The pacing frequency is controlled using a metronome set to 105 beats per minute (bpm) for 1.75 Hz and to 210 bpm for 3.5 Hz. Each test is repeated three times.

	Uncontrolled	Controlled	Reduction (%)
Walking at 1.75 Hz			
Peak acceleration (m/s^2)	0.41	0.16	70
MTVV(1) (m/s^2)	0.21	0.06	67
Running at 3.50 Hz			
Peak acceleration (m/s^2)	3.34	1.19	64
MTVV (m/s^2)	2.20	0.69	68

Table 4. Experimental performance assessment for walking and running excitation. (1) Maximum Transient Vibration value defined as the maximum value of 1s running RMS acceleration

The results are compared by means of the maximum peak acceleration and the MTVV computed from the 1 s running RMS acceleration. Table 4 shows the result obtained for the uncontrolled and controlled case. It is observed that the AMD designed (with a moving mass of 30 kg) performs well for both excitations, achieving reductions of approximately 70 %. Fig. 16 shows the response time histories (including the 1 s RMS) uncontrolled and controlled for a walking test. Fig. 17 shows the same plots for a running test.

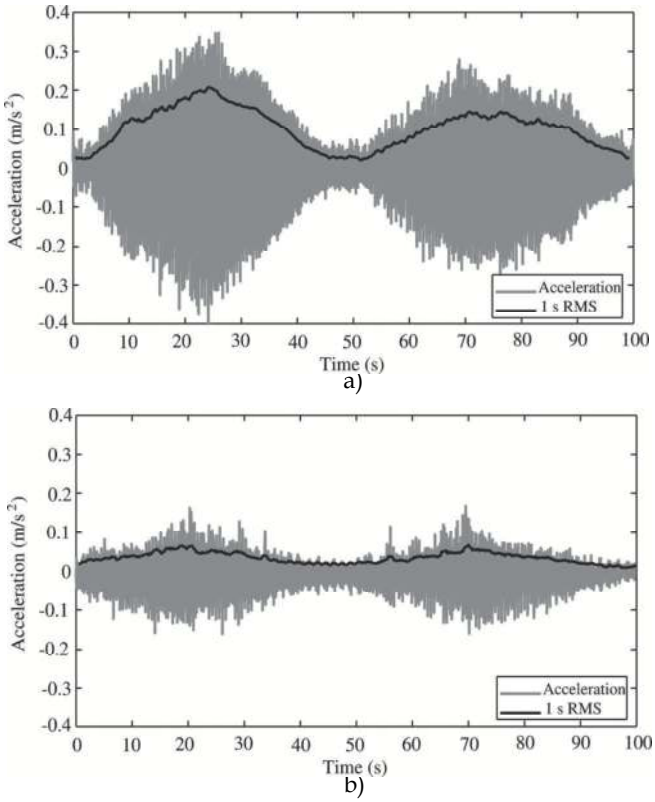

Fig. 16. Walking test on the footbridge. a) Uncontrolled $MTVV = 0.207\ m/s^2$. b) Controlled $MTVV = 0.067\ m/s^2$

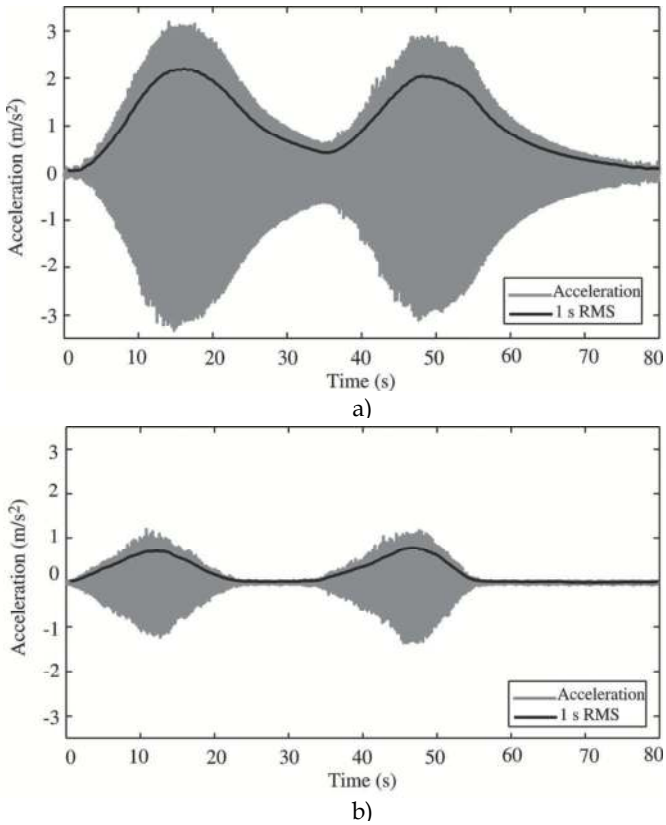

Fig. 17. Running test on the footbridge. a) Uncontrolled $MTVV = 2.198\ m/s^2$. b) Controlled $MTVV = 0.773\ m/s^2$

6. Conclusion

The active cancellation of human-induced vibrations has been considered in this chapter. Even velocity feedback has been used previously for controlling human-induced vibrations, it has been shown that this is not a desirable solution when the actuator dynamics influence the structure dynamics. Instead of using velocity feedback, here, it is used a control scheme base on the feedback of the acceleration (which is the actual measured output) and the use of a first-order compensator (phase-lag network) conveniently designed in order to achieve significant relative stability and damping. Note that the compensator could be equivalent to an integrator circuit leading to velocity feedback, depending on the interaction between actuator and structure dynamics. Moreover, the control scheme is completed by a phase-lead network to avoid stroke saturation due to low-frequency components of excitations and a nonlinear element to account for actuator overloading. An AVC system based on this control scheme and using a commercial inertial actuator has been tested on two in-service structures, an office floor and a footbridge.

The floor structure has a vibration mode at 6.4 Hz which is the most likely to be excited. This mode has a damping ratio of 3% and a modal mass of approximately 20 tonnes. Reductions of approximately 60 % have been observed in MTVV and cumulative VDV for controlled walking tests. For in-service whole-day monitoring, the amount of time that an R-factor of 4 is exceeded, which is a commonly used vibration limit for high quality office floor, is reduced by over 97 %. The footbridge has a vibration mode at 3.5 Hz which is the most likely to be excited. This mode has a damping ratio of 0.7 % and a modal mass of approximately 18 tonnes. Reductions close to 70 % in term of the MTVV has been achieved for walking and running tests.

It has been shown that AVC could be a realistic and reasonable solution for flexible lightweight civil engineering structures such as light-weight floor structure or lively footbridges. In these cases, in which low control forces are required (as compared with other civil engineering applications such as high-rise buildings or long-span bridges), electrical actuators can be employed. These actuators present advantages with respect to hydraulic ones such as lower cost, maintenance and level of noise. However, AVC systems for human-induced vibrations needs much further research and development to jump into building and construction technologies considered by designers. With respect to passive systems, such as TMDs, cost is still the mayor disadvantage. However, it is expected that this technology will become less expensive and more reasonable in the near future. Research projects involving the development of new affordable and compact actuators for human-induced vibration control are currently on the go (Research Grant EP/H009825/1, 2010).

7. Acknowledgment

The author would like to acknowledge the financial support of Universidad de Castilla-La Mancha (PL20112170) and Junta de Comunidades de Castilla-La Mancha (PPII11-0189-9979. The author would like to thank his colleagues Dr. Paul Reynolds and Dr Donald Nyawako from the University of Sheffield, and Mr Carlos Casado and Mr Jesús de Sebastián from CARTIF Centro Tecnológico for their collaboration in works presented in this chapter.

8. References

APS. *Instruction Manual Electro-Seis Model 400 Shaker*, APS Dynamics, USA, available from http://www.apsdynamics.com

Bachmann, H. (1992). Case studies of structures with man-induced vibrations. *Journal of Structural Engineering*, Vol.118, No.3, pp. 631-647, ISNN 0733-0445

Bachmann, H. (2002). Lively footbridges—a Real Challenge, *Proceedings of the International Conference on the Design and Dynamic Behaviour of Footbridges*, OTUA, Paris, France, November 20-22

Balas, M.J. (1979). Direct velocity feedback control of large space structures, *Journal of Guidance and Control*, Vol.2, No.3, pp. 252–53

Bolton, W. (1998). *Control engineering*, Logman, ISBN 978-0-582-32773-3, United Kingdom

Brownjohn, J.M.W., Pavic, A. & Omenzetter, P. (2004). A spectral density approach for modelling continuous vertical forces on pedestrian structures due to walking, *Canadian Journal of Civil Engineering*, Vol.31, No.1, pp. 65–77, ISSN 0315-1468

BS 6841. (1987). *Measurement and evaluation of human exposure to whole-body mechanical vibration and repeated shock*, British Standards Institution, ISBN 0-580-16049-1, United Kingdom

BS 6472. (2008*). Guide to evaluation of human exposure to vibration in buildings. Part 1: Vibration sources other than blasting*, British Standards Institution, ISBN 978-0-580-53027-2, United Kingdom

Caetano, E., Cunha, A., Moutinho, C. & Magalhães, F. (2010) Studies for controlling human-induced vibration of the Pedro e Inês footbridge, Portugal. Part 2: Implementation of tuned mass dampers, *Engineering Structures*, Vol.32, pp. 1082–1091, ISSN 0141-0296

Chung, L.Y. & Jin, T.G. (1998). Acceleration feedback control of seismic structures, *Engineering Structures*, Vol.20, No.1, pp. 62–74, ISSN 0141-0296

Díaz, I.M. & Reynolds, P. (2010a). On-off nonlinear active control of floor vibrations, *Mechanical Systems and Signal Processing*, 24: 1711–1726, ISSN 0888-3270

Díaz, I.M. & Reynolds, P. (2010b). Acceleration feedback control of human-induced floor vibrations, *Engineering Structures*, Vol.32, No.1, pp. 163–173, ISSN 0141-0296

Ebrahimpour, A. & Sack, R.L. (2005). A review of vibration serviceability criteria for floor structures, *Computers and Structures*, Vol.83, pp. 2488–94, ISSN 0045-7949

FIB-Bulletin 32. (2005). *Guidelines for the design of footbridges*, International Federation for Structural Concrete, Lausanne, Switzerland

Gómez, M. (2004). A new and unusual cable-stayed footbridge at Valladolid (Spain). *Steelbridge 2004: Symposium International sur les Ponts Metálliques*, Milau, France, June, pp. 23-25

Hanagan, L.M. & Murray, T.M. (1997) Active control for reducing floor vibrations, *Journal of Structural Engineering*, Vol.123, No.11, pp. 1497–1505, ISSN 0733-9445

Hanagan, L.M., Raebel, C.H. & Trethway, M.W. (2003a). Dynamic measurements of in-place steel floors to assess vibration performance, *Journal of Performance of Constructed Facilities*, Vol.17, pp. 126–135, ISSN - 0887-3828

Hanagan, L.M., Murray, T.M. & Premaratne, K. (2003b). Controlling floor vibration with active and passive devices, *The Shock and Vibration Digest*, Vol.35, No.5, pp. 347–65, ISSN 0583-1024

Hanagan, L.M. (2005). *Active floor vibration system*, United States Patent 6874748

Moutinho, C., Cunha, A. & Caetano, E. (2010). Analysis and control of vibrations in a stress-ribbon footbridge, *Structural Control and Health Monitoring*, doi: 10.1002/stc.390

Nyawako, D. & Reynolds, P. (2007) Technologies for mitigation of human-induced vibration in civil engineering structures, *The Shock and Vibration Digest*, Vol.36, No.(6), pp. 465–93, ISSN 0583-1024

Occhiuzzi, A., Spizzuoco, M. & Ricciardelli, F. (2008). Loading models and response control of footbridges excited by running pedestrians, *Structural Control and Health Monitoring*, Vol.15, pp. 349–368, ISSN 1545-2263

Pavic, A. & Willford, M. (2005). *Appendix G in Post-tensioned concrete floors design handbook–Technical Report 43*, Concrete Society, Slough, United Kingdom

Preumont, A. (1997). *Vibration Control of Active Structures: An introduction*, Kluwer Academic, Dordrecht, ISBN 1-4020-0496-9, The Netherlands

Reiterer, M. & Ziegler, F. (2006). Control of pedestrian-induced vibrations of long-span bridges, *Structural Control and Health Monitoring*, Vol.13, pp. 1003–1027, ISSN 1545-2263

Research Grant EP/H009825/1. (2010). *Active control of human-induced vibration*, PI: Dr Paul Reynolds, Engineering and Physical Sciences Research Council, 2010–2012, United Kingdom

Reynolds, P., Díaz, I.M. & Nyawako, D.S. (2009). Vibration testing and active control of an office floor, *Proceedings of the 27th International Modal Analysis Conference*, Orlando, Florida, USA

Setareh, M. & Hanson, R.D. (1992). Tuned mass damper to control floor vibration from humans, *Journal of Structural Engineering*, Vol.118, No.3, pp. 741–62, ISSN 0733-9445

Setareh, M. (2002). Floor vibration control using semi-active tuned mass dampers, *Canadian Journal of Civil Engineering*, Vol.29, No.1, pp. 76–84, ISSN 0315-1468

Slotine, J.J. & Li, W. (1991). *Applied non linear control*, Prentice-Hall, Chapter 5, ISBN 013-040890-5, USA

Wyatt, T.A. (1989). *Design guide on the vibration of floors*, The Steel Construction Institute, ISBN 1-870004-34-5, United Kingdom

Vibration Analysis and Control - New Trends and Developments
Edited by Dr. Francisco Beltran-Carbajal

ISBN 978-953-307-433-7
Hard cover, 352 pages
Publisher InTech
Published online 06, September, 2011
Published in print edition September, 2011

This book focuses on the important and diverse field of vibration analysis and control. It is written by experts from the international scientific community and covers a wide range of research topics related to design methodologies of passive, semi-active and active vibration control schemes, vehicle suspension systems, vibration control devices, fault detection, finite element analysis and other recent applications and studies of this fascinating field of vibration analysis and control. The book is addressed to researchers and practitioners of this field, as well as undergraduate and postgraduate students and other experts and newcomers seeking more information about the state of the art, challenging open problems, innovative solution proposals and new trends and developments in this area.

INTECH
open science | open minds

InTech Europe
University Campus STeP Ri
Slavka Krautzeka 83/A
51000 Rijeka, Croatia
Phone: +385 (51) 770 447
Fax: +385 (51) 686 166
www.intechopen.com

InTech China
Unit 405, Office Block, Hotel Equatorial Shanghai
No.65, Yan An Road (West), Shanghai, 200040, China
中国上海市延安西路65号上海国际贵都大饭店办公楼405单元
Phone: +86-21-62489820
Fax: +86-21-62489821